Surface Reactivity and Energetics of CH Radicals during Plasma Deposition of Hydrogenated Diamondlike Carbon Films

Jie Zhou and Ellen R. Fisher*

Department of Chemistry, Colorado State University, Fort Collins, Colorado 80523-1872

Received: June 30, 2006; In Final Form: August 23, 2006

The surface reactivity of CH radicals was measured during plasma deposition of hydrogenated diamondlike carbon (DLC) films using the imaging of radicals interacting with surfaces (IRIS) method. In this technique, spatially resolved laser-induced fluorescence (LIF) is used to determine surface reactivity, *R*, of plasma species. The measured reactivity of CH is near unity and shows no dependence on the applied rf power (*P*), argon fraction, substrate temperature, or substrate bias. Kinetic translational temperatures, Θ_T, of CH in the molecular beam were also measured. Modeling of the kinetic data yields Θ_T(CH) values of ∼2200−2500 K and 1600−1700 K for CH_4/Ar plasmas at pressures of 50 and 110 mTorr, respectively, with no clear dependence on the argon fraction (at $P = 100$ W). The average Θ_T(CH) does, however, change with *P*, $\Theta_T = \sim 2050-9050$ K, over the range $P = 180-20$ W. These results indicate that Θ_T(CH) is associated with the electron temperature in the plasma. The rotational temperature, Θ_R, determined from the CH rotational excitation spectrum is ∼1450 K with no clear dependence on *P* or the Ar fraction in the feed. The difference between Θ_T(CH) and Θ_R(CH) can be explained by the different relaxation rates after the dissociation of CH_4 by electron impact.

I. Introduction

Hydrogenated diamondlike carbon (DLC) films can be used in a wide range of applications because of high hardness, extremely low surface roughness, scratch resistance, chemical inertness, good thermal conductivity, high electrical resistance, and optical transparency.[1] There are several low-pressure methods that have been used to deposit DLC films, including microwave plasmas,[2,3] electron-cyclotron resonance (ECR) plasmas,[4,5] dc-arcjet discharges,[6,7] and inductively coupled plasmas (ICPs).[8,9] The material properties of films deposited by these techniques are usually dependent on the plasma parameters, which implies that different plasma species play a key role in film growth. Numerous studies have, therefore, been performed on plasma reactions and on the gas-phase densities of the different species in methane-based plasmas.[10−13] During the deposition processes, neutral hydrocarbon species are considered to be important precursors for film growth and have been widely studied.[14] Luque et al. have examined CH radicals in the CH $A^2\Delta \leftarrow X^2\Pi$ transition of a dc-arcjet discharge by laser-induced fluorescence (LIF).[15] Menningen and co-workers have used absorption spectroscopy to measure CH_3 concentrations in hot-filament and dc-discharge reactors.[16] The absolute concentration of C_2 has been measured by Kaminski et al. in a diamond CVD reactor by LIF.[17] Among these neutral species, CH_3 and CH_2 are thought to be the dominant contributors to DLC film growth, whereas the contribution of CH radicals to film formation is small because of its low flux in methane plasmas.[14,18] The quality of the film, however, can be greatly affected by CH radicals.[14] Therefore, data on the surface reactivity of CH radicals is very important to understand the mechanisms of film growth.

The roles of gas-phase radicals and gas−surface interactions during film growth processes are important to understand overall methane plasma chemistry. For example, Kuedell and co-workers have investigated the simultaneous interaction of CH_3 and H radicals with amorphous, hydrogenated carbon (a-C:H) films using optical in-situ diagnostics.[13,19] They found that the sticking coefficient of CH_3 radicals is related to the surface radical site or "dangling bond" density. These sites are created by H radicals through abstraction of surface hydrogen atoms. Impinging CH_3 radicals then adsorb at these active sites, leading to growth of a-C:H films. In contrast to CH_3, CH radicals have high reactivity (some reactions exhibit no activation barrier and, hence, occur even at low temperature) in the gas phase.[6,20] Furthermore, examination of the relevant literature indicates that CH is lost primarily through neutral chemistry with the parent methane molecules.[6] To date, however, there is little information about the relationship between the CH radicals and the quality of the deposited DLC films. Therefore, the measurements of CH reactivity with surfaces by our imaging of radicals interacting with surfaces (IRIS) technique will enable a better understanding of the mechanisms of DLC film growth in methane plasmas. We have previously published a limited set of data on CH surface reactivity;[21] here, we present a more complete description of the surface interactions of CH as a function of different plasma parameters.

The IRIS technique used in our laboratories provides a unique way to measure radical-surface interactions during plasma processing of a substrate.[22−25] It combines plasma molecular beam techniques with spatially resolved LIF to study the state-specific reactivity, as well as translational and rotational temperatures, of plasma-generated species during a plasma-processing event. With this method, the surface reactivity of radicals during plasma processing is directly measured by two-dimensional imaging using LIF. Moreover, the dependence of the surface reactivity on plasma parameters, substrate material, substrate temperature (T_S), and ion energy can also be obtained by this method because the use of a molecular beam facilitates independent variations of the plasma and surface conditions.

* To whom correspondence should be addressed. E-mail: erfisher@lamar.colostate.edu.

10.1021/jp064125n CCC: $33.50
Published on Web 10/06/2006

In addition, knowledge of the energy partitioning between different species is another important aspect to understanding the overall chemistry occurring in low-temperature plasmas. However, kinetic energy distributions of plasma species are difficult to determine.[26] IRIS not only allows us to obtain surface reactivity data but can also be used to measure the speed distributions of radicals in the plasma molecular beam[27−29] and of those scattered off of surfaces.[30,31] The average translational speed of radicals is determined by taking LIF images at different time delays after the laser excitation of the radicals and evaluating the spatial shift of the LIF images. This velocity can then be converted to a translational temperature, Θ_T. For example, we have measured both Θ_T and rotational temperature, Θ_R, for SiH in SiH_4/Ar and Si_2H_6/Ar plasmas. The results showed that Θ_R was ∼550 K and independent of applied rf power and gas composition, whereas Θ_T was significantly higher (∼1000 K) than Θ_R in SiH_4/Ar plasmas and independent of the argon fraction under the investigated range (<40%).[32] Interestingly, Θ_T in Si_2H_6/Ar plasmas was found to be close to Θ_R at a high argon fraction, suggesting that the initial high translational energy of SiH was thermalized to the internal SiH temperature via nonreactive collisions in the disilane systems. This was attributed to the lower probability of reaction between SiH and SiH_4 in the Si_2H_6 plasma.[32] Such studies have, therefore, allowed us to discern different mechanisms for energy partitioning and have provided valuable information on the relationship between the kinetic and rotational temperature of radicals in processing plasmas. In this study, Θ_T and Θ_R of CH, as a function of applied rf power and Ar fraction, were measured, and the results are discussed in terms of the energy partitioning in CH_4 plasmas.

II. Experiment

A. IRIS Apparatus. The IRIS apparatus has been described in detail previously.[22,23,25,30] Briefly, a combination of molecular beam techniques and LIF has been used to investigate the steady-state surface reactivity of gas-phase species during plasma processing of a substrate, as well as the gas-phase energetics of the species as a function of different plasma parameters, such as applied rf power (*P*), reactor source pressure, and gas composition. In a typical IRIS experiment, the feed gases enter the rear of a glass reactor tube; 13.56 MHz of rf power is applied to an inductor coil, and a plasma is produced. Expansion of the plasma through a series of collimating slits into a differentially pumped high-vacuum chamber generates an effusive molecular beam consisting of virtually all species present in the plasma, including the species of interest. The use of spatially and temporally resolved LIF allows the study of either the interaction of the radicals with surfaces or the velocity of the radicals in the molecular beam. For reactivity measurements, the LIF intensity of a freely expanding molecular beam is compared with the LIF intensity of a molecular beam that is directed onto a substrate. The difference in LIF intensity is directly proportional to the density of radicals scattered or created at the substrate's surface. For velocity measurements, "snapshots" of the LIF intensity of a freely expanding molecular beam are taken at different delay times after the laser excitation pulse. The velocity of radicals along the molecular beam axis can subsequently be deduced from the spatial movement in maximum intensity of the fluorescence between the different delays.

In the present work, the source of the molecular beam is a plasma consisting of either 100% CH_4 (General Air, 99.9%) or CH_4/Ar (General Air, 99.9%) mixtures with Ar fractions of 0−20%. For the mixtures, the gases are premixed before entering the reactor. The total gas flow is maintained at 30 sccm leading to a source pressure of 45−55 mTorr. (The pressure in the main chamber of the apparatus, where measurements are made, is ∼5 × 10^{-6} Torr during experiments.) The plasma is produced by the inductive coupling of 13.56 MHz of rf power (20−200 W) to an eight-loop induction coil surrounding the glass plasma reactor and tuned by a variable capacitor-matching network. The molecular beam was collimated by two slits, 1.08 and 1.23 mm wide, with the second slit 12 mm downstream from the first one.

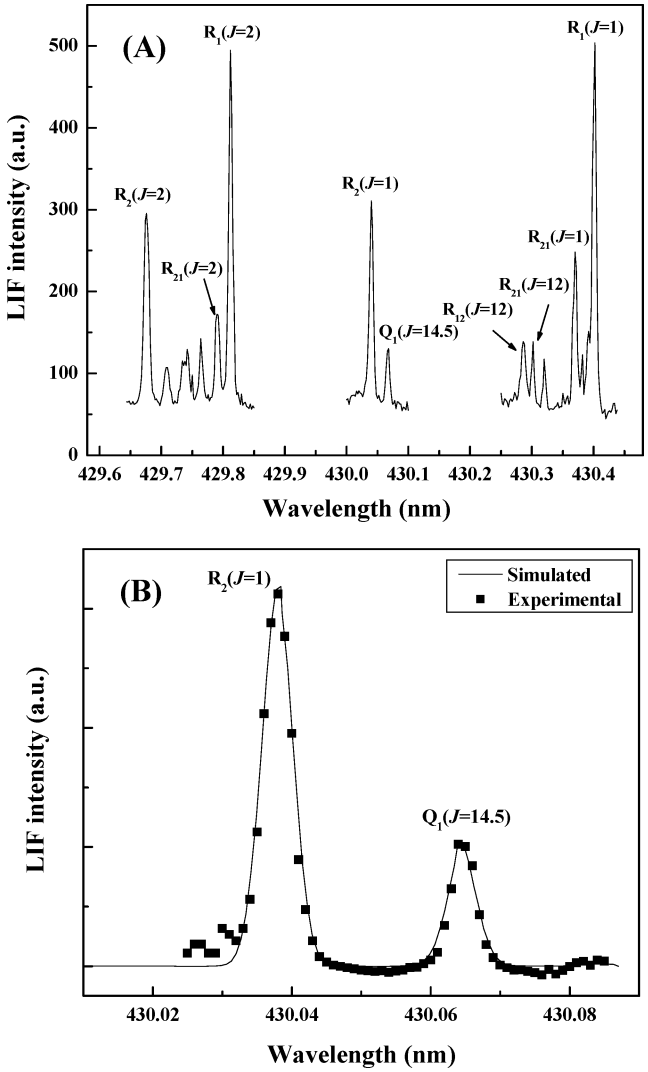

Figure 1. CH $A^2\Delta \leftarrow X^2\Pi$ excitation spectrum. (A) Long-range scan from 429.65 to 430.45 nm obtained using a 100% CH_4 plasma (50 mTorr, $P = 100$ W). The entire excitation spectrum was collected by three scans over different wavelength ranges. The $R_1(J = 1)$ was used for the IRIS reactivity and velocity measurements. (B) The portion of the experimental spectrum (closed squares) used for determining Θ_R-(CH) together with the simulated spectrum (solid line). In both figures, the λ doubling of the rotational lines is not resolved because of optical saturation of the transition.

A tunable excimer-pumped (Lambda Physik LPX210i, XeCl, 100 mJ/pulse, 100 Hz) dye laser system with Coumarin 440 (Exciton) intersects the plasma molecular beam at either 45 or 90° downstream from the plasma source and excites the CH $A^2\Delta \leftarrow X^2\Pi$ transition. For reactivity and velocity measurements, the laser was tuned to 430.404 nm (∼12 mJ/pulse), corresponding to the $R_1(J = 1)$ rotational line of the CH $A\ ^2\Delta \leftarrow X\ ^2\Pi$ transition (Figure 1A). A lens is used to focus the

laser radiation at the position of the molecular beam, yielding a well-defined laser beam <1 mm wide. All reactivity and velocity experiments were performed at laser energies in the optical saturation regime so that the measurements are not affected by small fluctuations in laser power.

Spatially and temporally resolved LIF signals are collected by an electronically gated, intensified charge-coupled device (ICCD) located perpendicular to both the molecular and the laser beam, directly above the interaction region. CH fluorescence is collected by a set of two lenses, with focal lengths of 300 and 75 mm, imaging a 2664 mm^2 area onto the 512 × 512 pixel array of the ICCD. An 8 nm bandwidth interference filter centered at 425 nm was placed between the ICCD camera and the vacuum chamber to reduce spurious signals from scattered laser light and plasma emission.

B. Reactivity Measurements. For reactivity measurements, the laser radiation is directed into the chamber so that it intersects the molecular beam at a 45° angle. A substrate (25 × 40 mm^2 p-type Si wafer with the polished side facing the molecular beam) can be rotated into the path of the molecular beam with its surface parallel to the laser beam. The laser−surface distance is maintained at ∼3 mm. Under the conditions used here, we estimate the total flux of molecules on the substrate to be $\sim 3 \times 10^{15}$ molecules cm^{-2} s^{-1}. Given that CH constitutes ∼7.3% of the dissociation products of CH_4,[6] we estimate the flux of CH radicals to be $\sim 2 \times 10^{14}$ molecules cm^{-2} s^{-1} (upper limit). LIF signals are collected with the surface out of and in the path of the molecular beam. Comparisons between the spatial distribution of scattered and incident molecules are used to determine the surface reactivity of the species of interest. A gate width of 2000 ns was used so that the fluorescence is collected over the entire radiative lifetime of the CH $A^2\Delta$ state (538 ± 5 ns).[33] The pixels were 4 × 4 binned to increase the signal-to-noise ratio. Each image consists of 6000 laser pulses. Multiple sets of data were taken with the surface alternating in and out of the molecular beam path. Background images were taken with the laser tuned to an off-resonance wavelength (430.2 nm) and subtracted from each image. Subsequently, the image with the surface out is subtracted from the image with the surface in, yielding the possible scatter or production of CH at the substrate surface. One-dimensional cross sections were formed by averaging 15 pixel columns along the laser axis and plotting signal intensity as a function of distance along the laser path.

Spatially resolved LIF data are interpreted using a quantitative model of the experiment that produces the surface reactivity of the CH radicals. The simulation program has been described in detail previously.[22,25] The model is based on the known geometry of the experiment and calculates the spatial distribution of the radical number density in the molecular beam at the interaction region, as well as the radical number density along the laser beam for molecules scattering from the substrate surface. The scattering coefficient, S, defined as the ratio of the flux of scattered molecules to that of the incident beam, is adjusted to best fit the experimental data. The surface reactivity, R, is defined as $1 - S$.

C. Velocity Measurements. In our IRIS experiments, the gas extraction is nearly effusive, which means that the measured velocity of CH in the molecular beam approximates the random velocity of CH in the plasma and that this can be used to study the kinetic translational temperature of CH in the plasma. For these measurements, the laser is directed into the high vacuum chamber so that it intersects the molecular beam at a 90° angle. To improve spatial and temporal resolution, the ICCD pixels are not binned and a short gate width of 100 ns is used. For higher accuracy, time delays are preferentially taken at the longest times possible. This is limited, however, by the radiative lifetime of CH (∼538 ns). Here, the ICCD images are collected at four different delays, typically 205, 705, 1205, and 1705 ns after the laser pulse for CH excitation. LIF signals of 5−8 accumulations of 6000 laser shots were acquired at each time delay. Background images obtained with an off-resonance laser wavelength were subtracted from the on-resonance images. One-dimensional cross section plots were made by averaging over 100 rows (10.08 mm) of pixels perpendicular to the laser beam and plotting signal intensity as a function of distance away from the laser beam path. This leads to snapshots of the spatial position of the LIF intensity at four different time delays.

Because only relatively short time delays could be used in these systems, the spatial movement at different time delays is not obvious. Therefore, to accurately determine the peak positions of LIF intensity, a symmetrical laser spatial profile is assumed, and the plot is fitted by a Gaussian function. As described previously,[23] the peak positions are then plotted as a function of time delay and fit with a linear regression. The slope of this linear fit yields the average velocity of CH along the center axis of the molecular beam.

D. Rotational and Translational Temperature Measurements. In our experiments, we measure the average speed of a particular molecule. One way to consider these measurements is to convert the speed to a translational temperature for comparison to internal degrees of freedom (i.e., rotational temperatures). In our work, we convert the average speeds to kinetic translational temperatures as noted above ($\Theta_T = \pi m v^2/8k$, where m is the mass of the radical and k is Boltzmann constant).[27,29] Note that the average velocity obtained by this method is considered to be a lower limit because radicals are also moving in radial directions. A Monte Carlo simulation program is used to simulate the spatial LIF intensity of CH along the molecular beam's central axis. This model assumes a Gaussian laser beam profile and a Maxwell−Boltzmann distribution of molecular velocities in the molecular beam. Although this latter assumption may not be entirely accurate for molecules in our plasma systems, we find that the distribution fits the data well, suggesting that this distribution can be characterized by a specific temperature for the molecule we are studying. Because of the nature of plasmas, the translational temperature we derive in this way may not be representative of other species temperatures but does offer a reasonable point of comparison to the rotational temperatures derived from the excitation spectra for the same species. The peak positions of the simulated data are plotted again as a function of time delay, and the slope is compared with the experimentally obtained value. The procedure is repeated at different Θ_T values until a best fit is obtained, yielding the final Θ_T(CH) value.

We have collected excitation spectra for CH over a wide range of wavelengths (429.6−430.5 nm),[21,34] Figure 1A, and have measured the rotational temperature using multiple lines from these spectra. This results in Θ_R values with fairly high errors because the amount of time it takes to collect the longer-range spectra can change the laser power sufficiently to move it out of the optical saturation regime. Moreover, these spectra are necessarily taken with larger-step sizes, making fitting of the spectra more difficult. Thus, for the purposes of determining Θ_R(CH) in this work, we focused on two rotational lines that have significantly different quantum states. Specifically, we used the relative heights and integrated areas of the neighboring R_2 ($J = 1$) and Q_1 ($J = 14.5$) rotational lines at 430.042 and

430.067 nm (Figure 1B). This relationship is sensitive to Θ_R because of the relatively large difference in the rotational quantum number. The use of two lines, such as these, in determining rotational temperatures from excitation spectra is not uncommon. These two lines are scanned in an excitation LIF spectrum with a step size of 0.001 nm in wavelength, and the LIF signal is collected for 1000 laser shots per step. For these experiments, ICCD was 4 × 4 binned; the gate delay with respect to CH excitation is 205 ns, and the gate width is 2000 ns. The final Θ_R is determined from simulations of the R_2 (J = 1) and Q_1 (J = 14.5) rotational lines using the LIFBASE program at different Θ_R values until a best fit to the experimental data is obtained.[35] Note that the LIFBASE program allows for spectra to be fit assuming linear, full, or partial saturation behavior. Although we operate in the optical saturation regime, as noted above,[28−31] the best fits to the experimental excitation spectra were found assuming a partial saturation in the simulation. This type of behavior has been seen previously and results when a laser beam interacts with a volume of gas that exceeds the volume of the focal point of the laser.[36]

III. Results

A. Spectroscopy. LIF is a nonintrusive and highly selective technique that allows for the identification and study of one type of species among many others in the plasma molecular beam. Figure 1A shows the CH excitation spectrum obtained in a 50 mTorr, 100% CH_4 plasma, which represents the CH $A^2\Delta \leftarrow X^2\Pi$ (0, 0) transition. The entire excitation spectrum was collected by three individual scans at different ranges, with a step size of 0.002 nm. Figure 1B shows the excitation spectrum of two closely spaced rotational lines, R_2 (J = 1) and Q_1 (J = 14.5), with significantly different quantum numbers. A comparison of the relative line intensities between the experimental spectrum and spectra simulated at different Θ_R yields Θ_R = 1460 ± 20 K for CH in the 50 mTorr, 100% CH_4 plasma at P = 100 W.

Figure 2A shows the CH LIF intensity as a function of P for 50 mTorr, 100% CH_4 plasmas. All CH LIF intensities were collected at the on-resonance wavelength, 430.402 nm [R_1(J = 1)]. The background LIF intensity obtained at the off-resonance wavelength (430.2 nm) was subtracted from the on-resonance LIF intensity to remove interference from plasma emission. As seen in Figure 2A, the CH LIF intensity increases almost linearly when P < 100 W. At P > 100 W, the CH LIF intensity reaches a saturation region. Increasing P to 160 and 180 W results in a small decrease in CH signal intensity. This trend contrasts with previous results obtained in fluorocarbon plasmas, in which the CF_2 LIF intensity increases continuously with increasing rf power.[37] It is, however, similar to results obtained for NH in NH_3 plasmas.[38]

B. Radical−Surface Interaction. Surface reactivity in IRIS experiments is measured by comparison of ICCD images obtained with the substrate surface in and out of the path of the plasma molecular beam. Figure 3 shows a typical set of 2-dimensional ICCD images of LIF signals for CH in a 50 mTorr, 100% CH_4 plasma at P = 140 W. The CH signals in the incident molecular beam are shown in Figure 3A. In Figure 3B, the substrate is rotated into the path of the molecular beam, and the LIF signal includes both CH in the incident molecular beam and any CH scattered from the substrate surface. Figure 3C is the difference between panels B and A in Figure 3, showing only signal from CH scattered from the surface. By averaging several columns of pixels along the laser beam axis, we produced the one-dimensional cross sections of the LIF images shown in Figure 3A and 3C, Figure 4. The simulation results, also shown in Figure 4, yielded S = 0.01 ± 0.04, which results in a surface reactivity of R = 0.99 ± 0.04 at the surface of a depositing a-C:H film.

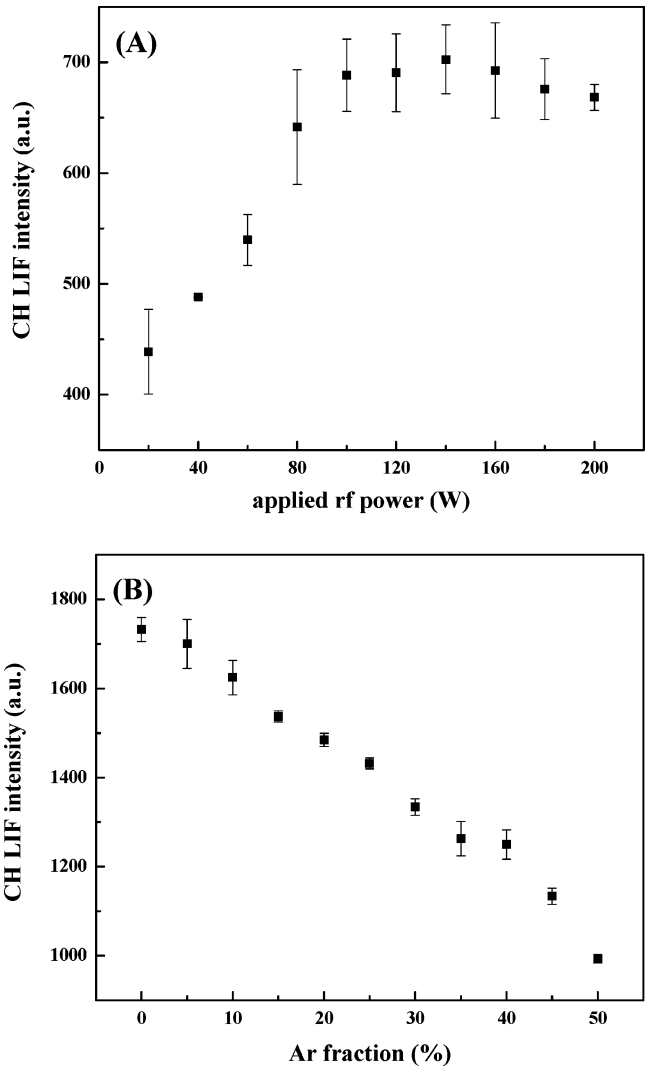

Figure 2. Mean CH LIF intensity for (A) a 100% CH_4 plasma at 50 mTorr as a function of applied rf power and (B) a CH_4/Ar plasma at 50 mTorr as a function of Ar fraction in the feed. Uncertainties in these values are represented by vertical error bars that are one standard deviation of the mean of several measurements ($n \geq 3$).

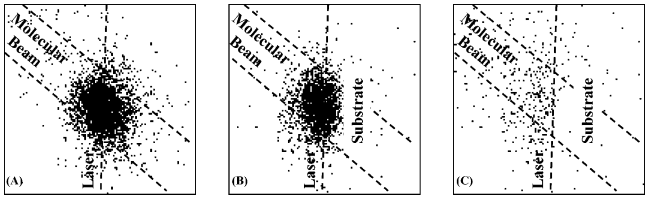

Figure 3. Two-dimensional ICCD images of CH LIF signals in (A) a 140 W, 100% CH_4 plasma molecular beam and (B) with a Si substrate rotated into the path of the molecular beam at a laser-surface distance of 3 mm. Image C is the difference between images A and B and shows only the LIF signal arising from CH radicals scattered off the surface. Dashed lines indicate the locations of the molecular beam and the laser beam.

The effects of P, T_S, substrate bias, and Ar fraction on the surface reactivity of CH have been measured, and the resulting R values are listed in Table 1. As can be seen clearly from these data, the surface reactivity of CH is nearly unity and independent of these parameters. This high surface reactivity of CH implies

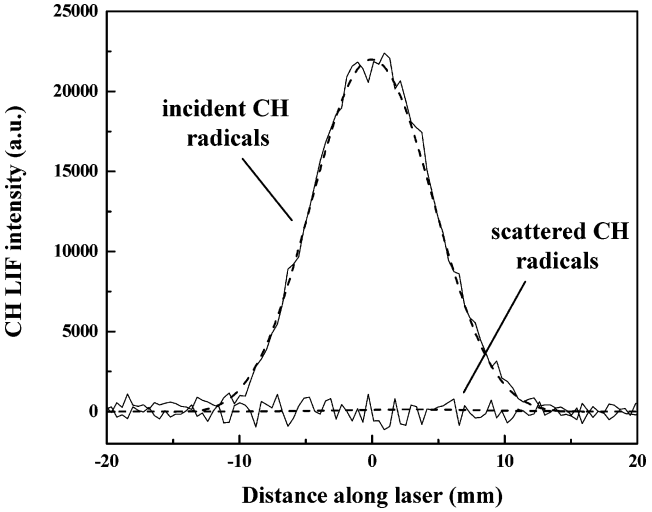

Figure 4. Cross-sectional data of the CH IRIS images presented in Figure 3. LIF signals are shown for radicals in the molecular beam incident on the substrate and for radicals scattering from the substrate (corresponding to parts A and C of Figure 3, respectively). Dashed lines are simulated curves as obtained by the reactivity simulation program described in the text, yielding $S = 0.01 \pm 0.04$. This corresponds to a surface reactivity for CH of $R = 0.99 \pm 0.04$.

TABLE 1: Surface Reactivity (*R*) Values for CH

source gases	argon fraction (%)	applied rf power (W)	substrate temp (K)	substrate bias (V)[a]	reactivity[b]
CH_4	0	80	298	−	0.99 ± 0.05
	0	100	298	−	0.98 ± 0.03
	0	120	298	−	1.00 ± 0.04
	0	140	298	−	0.99 ± 0.04
	0	160	298	−	0.98 ± 0.06
	0	100	311	−	0.97 ± 0.05
	0	100	363	−	1.00 ± 0.06
	0	100	433	−	0.99 ± 0.05
	0	100	503	−	0.97 ± 0.03
	0	100	573	−	1.00 ± 0.06
	0	100	298	400	0.98 ± 0.04
	0	100	298	200	0.99 ± 0.05
	0	100	298	−200	0.99 ± 0.05
	0	100	298	−400	0.98 ± 0.06
CH_4/Ar	5	100	298	−	1.00 ± 0.05
	10	100	298	−	0.99 ± 0.04
	15	100	298	−	0.96 ± 0.07
	20	100	298	−	0.99 ± 0.05

[a] A dash indicates the substrate was not biased for these experiments. [b] These values represent the mean of several data sets ($n \geq 3$). Errors represent one standard deviation of the mean.

that almost all incident CH radicals have been lost at the surface, either via a simple adsorption (sticking reaction), an abstraction of a surface atom, or recombination with another radical at the surface. This is discussed further below.

C. Translational and Rotational Temperatures. A representative velocity measurement is shown in Figures 5 and 6 for CH in a CH_4/Ar plasma (Ar fraction = 10% and $P = 100$ W), using four different time delays and a 90° geometry between the laser and molecular beam. Figure 5 shows the ICCD images, and Figure 6 shows the corresponding cross-sectional LIF signals. As the time delay increases, the intensity of the LIF signal decreases and the cross-section LIF signal shifts along the direction of the molecular beam. The shift is more clearly seen in the inset of Figure 6, which shows the peak position of LIF intensity as a function of time delay. The LIF intensity decreases with increasing time delay as a result of the radiation decay of the excited CH A $^2\Delta$ state after the laser-excitation pulse. As noted above, larger steps in the time delay are preferred for more accurate measurement, but this is limited by the relatively low signal-to-noise ratio at longer time delays. The time delay steps (500 ns) used in the velocity measurements are nearly as long as the radiative lifetime of CH. The good agreement between the experimental and simulated cross sections in Figure 6 indicates the CH radicals in the effusive molecular beam follow a Maxwell−Boltzmann distribution. The simulation yields an average velocity, v, of 1960 ± 40 m/s, corresponding to $\Theta_T = 2520 \pm 120$ K under these plasma conditions.

Figure 7 shows the average kinetic velocity of CH as a function of P and the Ar fraction. For the measurement of P dependence, 100% CH_4 was used, and the pressure was kept at 50 mTorr. As shown in Figure 7A, very high average kinetic velocities of CH were found at low P (20 and 60 W). Above 100 W, no significant change in the average kinetic velocities can be seen with further increasing P. This rapid decrease in velocity at high P is concomitant with a transition of the CH_4-containing plasmas from a low-density regime to a high-density regime. Our previous work showed there are two significant regimes in our inductively coupled plasma reactor: (1) a capacitive E mode with low plasma density, high electron temperature, and (2) an inductive coupling H mode with high plasma density, low electron temperature.[32] Figure 7B shows the effects of Ar addition on the speed of CH radicals at different pressures, 50 and 110 mTorr with $P = 100$ W. No significant dependence of the Ar fraction on the average kinetic velocity of CH can be found under the investigated Ar fraction range at both pressures. However, a decrease in the average kinetic velocity of CH radicals can be seen at the higher pressure. This might indicate lower electron temperatures in the plasma at higher pressure.

The average CH kinetic translational temperatures are given as a function of P and the Ar fraction in Figure 8. At low P, 20 and 60 W, Θ_T values are 9050 ± 2360 and 4270 ± 1290 K, respectively. At $P \geq 100$ W, no significant dependence of Θ_T ($\sim$2050−2300 K) on P was measured. Θ_T values at different Ar fractions and pressures are shown in Figure 8B. No clear dependence of Θ_T(CH) on the Ar fraction can be observed. However, Θ_T is significantly lower at the higher source pressure of 110 mTorr.

Figure 8 also shows Θ_R(CH) determined as described above (Figure 1B). As can be seen, Θ_R is nearly independent of P, the Ar fraction, and pressure, indicating that the rotational energy of CH radicals has been thermalized. Filippov et al. have calculated that the rotation relaxation coefficient of CH is $\sim 1.6 \times 10^{-10}$ cm^3/s.[39] A comparison of this relaxation rate with the chemical reaction rate of 1×10^{-10} cm^3/s for reaction 5 shows that CH can easily be rotationally equilibrated via several nonreactive collisions before reacting with CH_4 molecules.[12,40] Note that Brown et al. have indicated that rotational equilibrium can be achieved for diatomic molecules in four to six collisions.[6]

IV. Discussion

Characterization of plasma chemistry, species, and gas temperatures are complicated by the array of different species and possible reactions present in the system. Thus, it is difficult to measure a system temperature because the plasma contains a variety of species each with a different mass and electrical nature.[41] Consequently, each species may have its own characteristic temperature which may or may not be in thermal equilibrium with other species in the plasma.[41] The energy distribution for plasma species is, however, largely controlled

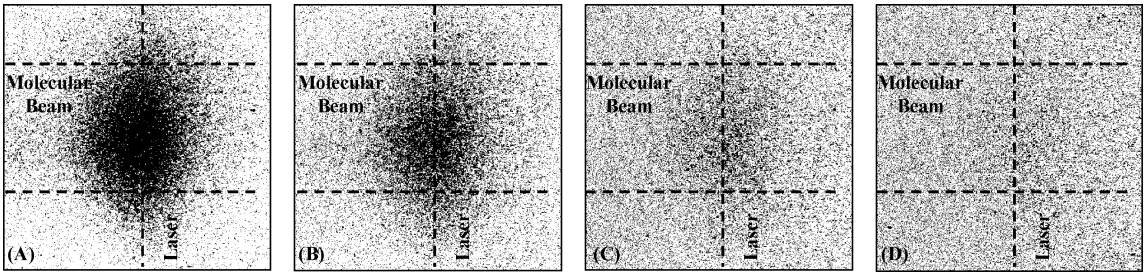

Figure 5. ICCD images of LIF signals for CH radicals in a 50 mTorr, CH_4/Ar (Ar fraction = 10% and P = 100 W) plasma molecular beam at four different gate delays: (A) 205, (B) 705, (C) 1205, and (D) 1705 ns after laser excitation. Dashed lines indicate the locations of the molecular beam and the laser beam, which intersect at a 90° angle.

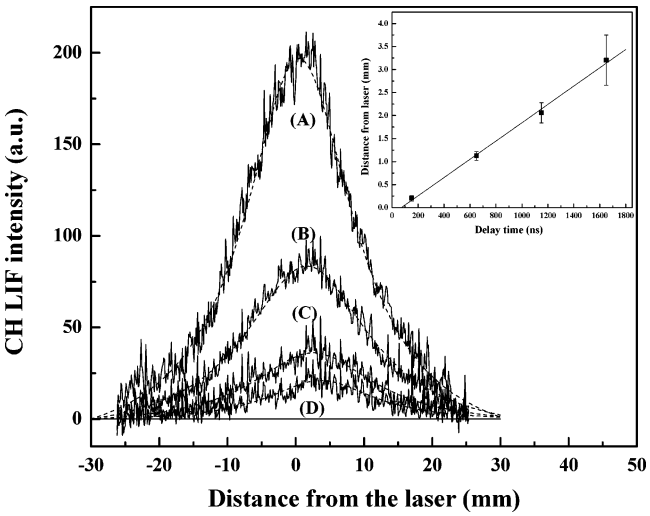

Figure 6. Cross-sectional data for the CH LIF images shown in Figure 5 (solid lines) at four different time delays: (A) 205, (B) 705, (C) 1205, and (D) 1705 ns after laser excitation. Simulated curves for Θ_T(CH) = 2520 ± 120 K are also shown (dashed lines). In the inset, the spatial positions of the maxima of the LIF signals are plotted as a function of time delay. The slope (1960 ± 40 m/s) of the linear regression corresponds to the velocity of CH in the direction of the central axis of the molecular beam, a lower limit to the CH velocity in the molecular beam.

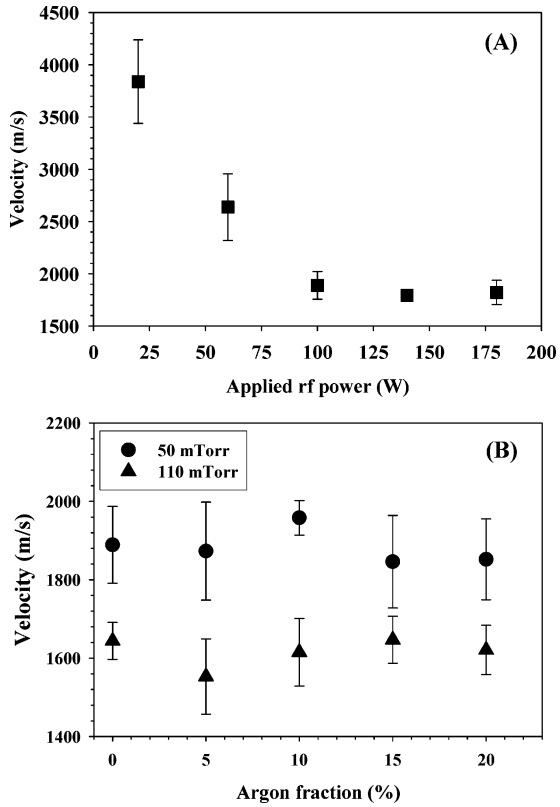

Figure 7. Velocity of CH in plasma molecular beams of (A) 50 mTorr, 100% CH_4 plasmas as a function of P and (B) 50 mTorr and 110 mTorr CH_4/Ar plasmas (P = 100 W) as a function of the Ar fraction in the feed. Errors represent one standard deviation of the mean.

by their formation mechanisms. Thus, to explain the power dissipation (as measured by internal and kinetic temperatures of CH) and the observed CH LIF intensity variation with P observed here, Figure 2, the creation and loss mechanisms of CH in CH_4 plasmas need to be addressed.

In CH_4 plasmas, CH is created primarily by direct electron-impact dissociation reactions of CH_4, reactions 1 and 2 (the threshold energies for these two reactions are 9.19 and 13.71 eV, respectively),[6,10]

$$CH_4 + e \rightarrow CH + H + H_2 + e \quad (1)$$

$$CH_4 + e \rightarrow CH + 3H + e \quad (2)$$

rather than through a sequential dissociation of CH_3 or CH_2, as shown in reaction 3. There are two loss channels for CH radicals,

$$CH_x\ (x = 2, 3) + e \rightarrow CH + H\ (H_2) + e \quad (3)$$

gas-phase reactions and surface loss reactions. For the gas-phase loss channel, under the present discharge conditions, two reactions are important, processes 4 and 5.

$$CH + H \rightarrow C + H_2 \quad (4)$$

$$CH + CH_4 \rightarrow H + C_2H_4 \quad (5)$$

Reactions 4 and 5 have no activation barriers; hence, they occur even in a cool-discharge environment with high reaction rates, 3×10^{-10} and 1×10^{-10} cm^3/s, respectively.[6] Furthermore, considering the low density of H relative to that of CH_4 in CH_4 plasmas, reaction 5 should be the primary loss channel for CH radicals in the gas phase. As shown in the results section, CH radicals demonstrated near-unity surface reactivity, suggesting that the primary surface loss mechanism is reaction 6

$$CH + \text{surface} \rightarrow \text{product} \quad (6)$$

Assuming that creation and loss of CH radicals are in equilibrium and ignoring reactions 2 and 4, a balance equation for CH radicals can be written as

$$k_c[CH_4]n_e = k_{lg}[CH][CH_4] + k_{ls}[CH]A_s \quad (7)$$

where k_c, k_{lg}, and k_{ls} are the rate constants for the CH creation reaction 1, the CH gas-phase loss reaction 5, and the CH surface loss reaction 6, respectively, n_e is the electron density in the plasma, and A_s is the inner surface area of the plasma reactor.

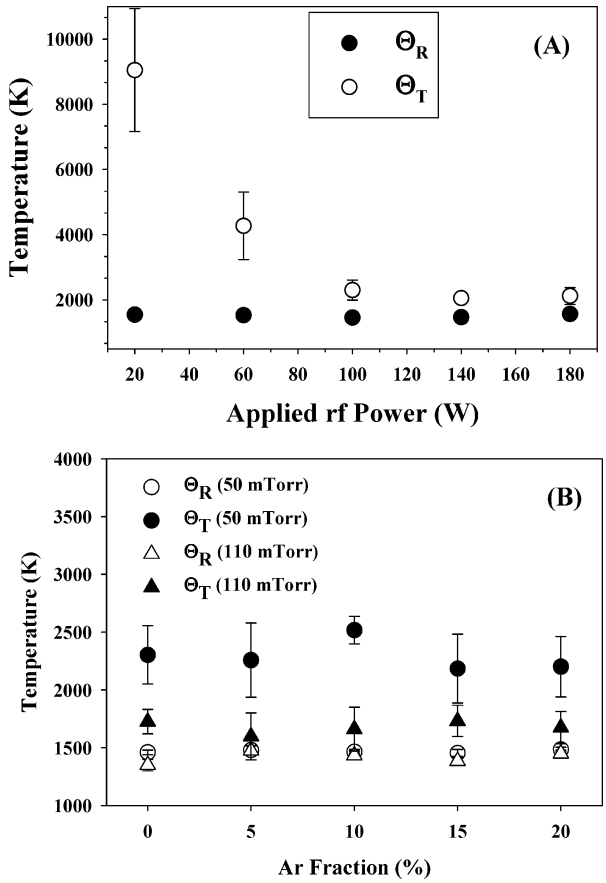

Figure 8. Average kinetic temperature, Θ_T, and rotational temperature, Θ_R, of CH in (A) 50 mTorr, 100% CH_4 plasmas as a function of *P* and (B) CH_4/Ar plasmas ($P = 100$ W) at 50 mTorr and 110 mTorr as a function of the Ar fraction. Θ_T values correspond to the velocities in Figure 7. Errors represent one standard deviation of the mean.

Note that n_e is proportional to *P* under our conditions ($n_e = kP$), which has been confirmed by previous Langmuir probe results.[32] Equation 7 also can be rewritten as eq 8. Here, $[CH_4]$

$$[CH] = \frac{k_c[CH_4]n_e}{k_{lg}[CH_4] + k_{ls}A_s}$$

is also a function of *P* and decreases with increasing *P* because the methane plasmas are highly depositing systems. As *P* is increased, the degree of CH_4 dissociation will increase because of the increase in electron density, yielding a higher deposition rate. Consequently, CH_4 density decreases during the residence period in the plasma reactor because of the deposition loss of hydrocarbon radicals or ions, which are produced via the dissociation reactions of CH_4 molecules by electron impact. The accurate description of $[CH_4]$ as a function of *P* will not be discussed here because of its complexity. At low *P* ($k_{lg}[CH_4] \gg k_{ls}A_s$ because of the low dissociation rate of CH_4 and high $[CH_4]$), eq 8 can be expressed as $[CH] = kP$, which corresponds to the linear region in Figure 2A. For $100 < P < 180$ W, [CH] is maximized because the increase in [CH], as a result of higher n_e, has been counteracted by the decrease in $[CH_4]$ because of film deposition. At $P > 180$ W, the increase in [CH] from higher n_e cannot compensate for the loss of $[CH_4]$ through film deposition. Thus, a small decrease in [CH] can be seen in this region, although it is still within experimental error. The CH LIF intensity decreases monotonically as a function of Ar fraction for 50 mTorr CH_4/Ar plasmas at $P = 100$ W, Figure 2B, as expected from the decrease in CH_4 concentration in the mixture.

One additional consideration in the examinination of the CH radical density measurements in CH_4 plasmas is the average dissipated energy per molecule of precursor gas, the Yasuda parameter, *Y*, which can be roughly determined for a given reactor system with a single monomer by the ratio of input power to gas flow.[42] For the conditions employed here, *Y* varies from ~9 eV at 20 W to ~93 eV at 200 W. Thus, at low *P*, CH production will be limited by the available energy per CH_4 molecule. At $P = 100$ W ($Y \approx 46$ eV), the CH_4 molecules are essentially consumed through film deposition (i.e., $[CH_4]$ is extremely low) such that CH production at $P > 100$ W is limited by the available CH_4 molecules.

The surface reactivity of CH is near unity and independent of all experimental variables studied, suggesting CH production via ion bombardment of a-C:H films or via surface reactions of other species are clearly negligible. The mechanism for surface loss is, therefore, of significant interest. The growth mechanisms of hydrogenated carbon films can help elucidate this. It is well-known that in methane-containing plasmas, CH_3 and CH_2 radicals have a higher gas-phase density and, therefore, are considered to be the primary contributors to film growth.[10,14] Morrison and co-workers have reported that 48.5 and 42.2% of the total dissociation reactions of CH_4 contribute to the creation of CH_3 and CH_2, respectively, whereas only 4.4% contribute to the creation of CH.[10] Tachibana et al. also reported that the calculated deposition rate contributed by CH radicals is smaller than the observed deposition rate by 2 orders of magnitude.[14] The film growth is, therefore, primarily controlled by the following processes: (1) the abstraction of H atoms from C−H bonds on the surface by H radicals, creating H_2(g) and active sites on the surface, and (2) the adsorption of CH_3 and CH_2 radicals at these active sites, resulting in film growth.

Here, we propose the following mechanisms about the surface interactions of CH radicals; note no CH desorption processes are proposed because of the negligible scattered signals observed in our IRIS experiments.

As shown in reaction 9, CH radicals may react with the active

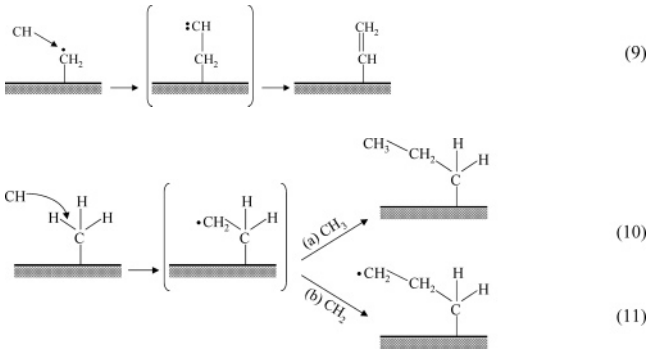

sites on the surface to form intermediate radicals, which subsequently convert to stable C_2 products. The probability of CH surface loss via reaction 9 clearly depends on the surface density of active sites. From the literature, the surface coverage percentages of sp^3-CH groups, sp^2-CH groups, and dangling bonds on the surface of an a-C:H film are ~95, <1, and ~4%, respectively.[43] This suggests that the surface loss of CH radicals via reaction 9 occurs with low probability because of the low density of active sites on the surface of a-C:H films. Alternatively, CH radicals may react with C−H bonds on the surface via reactions 10 and 11 because of a high concentration of C−H bonds on the surface of an a-C:H film. Considering the high reactivity rate of CH radicals with H_2 in the gas phase via CH + H_2 → CH_2 + H (rate coefficient is 2.01×10^{-10} cm^3/s)[44]

and the lower bond energy of C−H (413 kJ/mol) than that of H−H (436 kJ/mol),[45] we can reasonably speculate that reactions 10 and 11 can occur with high probability on the surface, although there are no direct kinetic data for these reactions. The intermediate C_2 active sites can quickly be filled via reactions with gas-phase CH_3 and CH_2, resulting in film growth. From this discussion, CH is clearly involved in film growth despite its low gas-phase density.

Knowledge of energy partitioning between different plasma species is important to an overall understanding of the chemistry occurring in low-temperature plasmas. It is commonly accepted that the average rotational temperature of gas-phase species (including stable species, as well as transient species such as radicals) is equal to the average gas temperature.[46−49] The results presented here, however, are in apparent disagreement with this assumption because Θ_T is considerably higher than Θ_R for CH in methane plasmas. During the dissociation process by electron impact reactions, the electron energy is used to dissociate precursor molecules, and the released excess energy is transferred to the dissociated fragments. Thus, high initial translational and rotational energies for these fragments can be obtained from the high electron energy. As observed here, Θ_R is independent of *P*, the Ar fraction, and pressure, which indicates that the high initial-rotational temperatures have been reduced because of the high rotational-relaxation rate for CH. The Θ_T values measured for CH in 100% CH_4 and CH_4/Ar plasmas are, however, significantly higher than Θ_R (this is more obvious at low pressure), which suggests that the initial high translational energy is not equilibrated with the internal temperature of the CH radicals prior to extraction from the plasma reactor.

In Figure 8A, the two very high Θ_T values, obtained at the lowest *P*, are likely related to higher electron temperatures in this low-power regime. This has been confirmed by our previous diagnostic data in the CH_4/Ar plasmas by Langmuir probe.[32] In that study, we also found that the electron temperature, T_e, is nearly constant in the high-power regime. The variation in Θ_T can, therefore, be explained by the change in T_e in the plasma. Moreover, the lower Θ_T values at the higher pressure, Figure 8B, are consistent with this assumption because T_e usually decreases with increasing pressure.[26] Although there are no direct data available on translational relaxation rates for CH created by electron-impact dissociation of CH_4, the data obtained here indirectly support another assumption, the one that the relaxation rate of the translational energy is much lower than that for rotational energy and the reaction rate between CH and CH_4. Considering the high reaction rate with CH_4 in the gas phase, we find that the CH radicals probed in the molecular beam are produced relatively close to the extraction orifice. Radicals with higher Θ_T will have fewer collisions than colder CH in the amount of time it takes for them to escape the plasma source. As a consequence, the CH that survives and is extracted into the molecular beam could be relatively hot. These CH radicals would also have less opportunity for full equilibration of the translational and internal degrees of freedom. Ar addition to the plasma increases the probability of thermalizing collisions. As can be seen in Figure 8B, however, the CH translational energy was still not thermalized to the internal CH temperature (Θ_R) even when the gas mixture contained 20% Ar. Unfortunately, the further increase of the argon fraction in CH_4/Ar mixtures is limited by the significant decrease of CH signal at higher Ar fractions. In a previous study, we measured Θ_T for SiH in Si_2H_6/Ar plasmas as a function of argon fraction.[32] We found that Θ_T(SiH) decreased significantly with increasing argon fraction because the added Ar decreased the probability of a chemical reaction between SiH and SiH_4, as a result of the decrease in SiH_4 density in Si_2H_6/Ar plasmas with increasing argon fraction. Hence, although not strictly parallel to the present system, these results indicate that the initial high translational energy still can be relaxed via nonreactive collisions.

V. Summary

The surface reactivity of CH radicals produced in CH_4/Ar plasmas as a function of various parameters, including *P*, the Ar fraction, T_S, and substrate bias has been measured by the IRIS technique. A surface reactivity of nearly unity has been determined for CH under all conditions studied. This very high reactivity suggests that the CH radical has a significant influence on the properties of the a-C:H films, despite its relatively low gas-phase density in CH_4 plasmas. In addition, the kinetic translational temperature and the rotational temperature of CH were measured. Θ_R is essentially independent of *P* and gas composition, which indicates that the rotational energy of CH radicals is cooled because of the high rotational-relaxation rate. Θ_T values are, however, considerably higher than Θ_R, especially at low source pressures, suggesting the thermodynamic equilibrium for Θ_T has not been established in these systems. The high initial Θ_T(CH) is likely a result of the excess energy released in the electron impact dissociation process of CH_4 and is also associated with the electron temperature in the plasma.

Acknowledgment. Financial support for this work was provided by the National Science Foundation (NSF-0137664). We also gratefully acknowledge Dr. Jorge Luque and Dr. Dongping Liu for helpful suggestions and discussions.

References and Notes

(1) Haverkamp, J.; Mayo, R. M.; Bourham, M. A.; Narayan, J.; Jin, C.; Duscher, G. *J. Appl. Phys.* **2003**, *93*, 3627.
(2) Choi, W. S.; Chung, I.; Lee, Y. Z.; Hong, B. *Surf. Coat. Technol.* **2004**, *180−181*, 254.
(3) Umehara, Y.; Murai, S.; Koide, Y.; Murakami, M. *Diamond Relat. Mater.* **2002**, *11*, 1429.
(4) Lung, B. H.; Chiang, M. J.; Hon, M. H. *Thin Solid Films* **2001**, *392*, 16.
(5) Ueng, H. Y.; Guo, C. T. *Appl. Surf. Sci.* **2005**, *249*, 246.
(6) Brown, M. S.; Forlines, R. A.; Ganguly, B. N. *J. Appl. Phys.* **2005**, *97*, 103302.
(7) Tang, W.; Liu, J.; Huang, T.; Lu, F. *Diamond Relat. Mater.* **2001**, *10*, 327.
(8) Sun, Z.; Xu, S.; Ostrikov, K. N. *Diamond Relat. Mater.* **2002**, *11*, 92.
(9) Lee, J. J. *Surf. Coat. Technol.* **2005**, *200*, 31.
(10) Morrison, N. A.; William, C.; Milne, W. I. *J. Appl. Phys.* **2003**, *94*, 7031.
(11) Yamashita, Y.; Toyoda, H.; Sugai, H. *Jpn. J. Appl. Phys.* **1989**, *28*, 1647.
(12) Brinkman, E. A.; Raiche, G. A.; Brown, M. S.; Jeffries, J. B. *Appl. Phys. B* **1997**, *64*, 689.
(13) Hummernbrum, F.; Kempkens, H.; Ruzicka, A.; Sauren, H. D.; Schiffer, C.; Uhlenbuschl, J.; Winter, J. *Plasma Sources Sci. Technol.* **1992**, *1*, 221.
(14) Tachibana, K.; Mukai, T.; Yuuki, A.; Matsui, Y.; Harima, H. *Jpn. J. Appl. Phys.* **1990**, *29*, 2156.
(15) Luque, J.; Juchmann, W.; Jeffries, J. B. *Appl. Opt.* **1997**, *36*, 3261.
(16) Menningen, K. L.; Chids, M. A.; Toyoda, H.; Ueda, Y.; Anderson, L. W.; Lawler, J. E. *Contrib. Plasma Phys.* **1995**, *35*, 359.
(17) Kaminski, C.; Ewart, P. *Appl. Phys. B* **1995**, *61*, 585.
(18) Yun, J.; Dandy, D. S. *Diamond Relat. Mater.* **2005**, *14*, 1432.
(19) Keudell, A. V.; Meier, M.; Schwarz-Selinger, T.; Jacob, W. *J. Appl. Phys.* **2001**, *89*, 2979.
(20) Thiesemann, H.; MacNamara, J.; Taaties, C. A. *J. Phys. Chem. A* **1997**, *101*, 1881.
(21) Liu, D.; Martin, I. T.; Zhou, J.; Fisher, E. R. *Pure Appl. Chem.* **2006**, *78*, 1187.
(22) Fisher, E. R. *Plasma Process. Polym.* **2004**, *1*, 13.
(23) Zhang, J.; Williams, K. L.; Fisher, E. R. *J. Phys. Chem. A* **2003**, *107*, 593.

(24) Zhang, J.; Fisher, E. R. *J. Phys. Chem. B* **2004**, *108*, 9821.
(25) Williams, K. L.; Fisher, E. R. *J. Vac. Sci. Technol. A* **2003**, *21*, 1024.
(26) Lieberman, M. A.; Lichtenberg, A. J. *Principles of Plasma Discharges and Material Processing*; Wiley and Sons: New York, 1994.
(27) McCurdy, P. R.; Venturo, V. A.; Fisher, E. R. *Chem. Phys. Lett.* **1997**, *274*, 120.
(28) Bogart, K. H. A.; Cushing, J. P.; Fisher, E. R. *J. Phys. Chem. B* **1997**, *101*, 10016.
(29) Kessels, W. M. M.; McCurdy, P. R.; Williams, K. L.; Barker, G. R.; Venturo, V. A.; Fisher, E. R. *J. Phys. Chem. B* **2002**, *106*, 2680.
(30) McCurdy, P. R.; Butoi, C. I.; Williams, K. L.; Fisher, E. R. *J. Phys. Chem. B* **1999**, *103*, 6919.
(31) Butoi, C. I.; Steen, M. L.; Peers, J. R. D.; Fisher, E. R. *J. Phys. Chem. B* **2001**, *105*, 5957.
(32) Zhou, J.; Zhang, J.; Fisher, E. R. *J. Phys. Chem. A* **2005**, *109*, 10521.
(33) Becker, K. H.; Brenig, H. H.; Tatarczyk, T. *Chem. Phys. Lett.* **1980**, *71*, 242.
(34) Zhou, J. Diagnostics of Carbon and Silicon-based Plasmas: From Surface Chemistry to Gas-Phase Physics. Ph.D. Thesis, Colorado State University, Fort Collins, CO, 2006.
(35) Luque, J.; Crosley, D. R. *LIFBASE: Database and Spectral Simulation*, 2.0.54 ed.; SRI International Report MP 99-009; SRI International: Menlo Park, CA, 2005.
(36) Ho, P.; Breiland, W. G.; Buss, R. J. *J. Chem. Phys.* **1989**, *91*, 2627.
(37) Martin, I. T.; Fisher, E. R. *J. Vac. Sci. Technol. A* **2004**, *22*, 2168.
(38) Steen, M. L.; Kull, K. R.; Fisher, E. R. *J. Appl. Phys.* **2002**, *92*, 55.
(39) Filippov, A. V.; Mankelevich, Y. A.; Pal, A. F.; Rakhimova, T. V.; Ryabinkin, A. N.; Serov, A. O.; Yuriev, A. Y. Presented at the 17th International Symposium on Plasma Chemistry, Toronto, Canada, 2005.
(40) Luque, J.; Crosley, D. R. *J. Chem. Phys.* **1996**, *104*, 2146.
(41) Grill, A. *Cold Plasmas in Materials Fabrication*; IEEE Press: Piscataway, NJ, 1994.
(42) Yasuda, H. *Plasma Polymerization*; Academic Press: Orlando, FL, 1985.
(43) Keudell, A. V.; Meier, M.; Schwarz-Selinger, T. *Appl. Phys. A* **2001**, *72*, 551.
(44) Fulle, D.; Hippler, H. *J. Chem. Phys.* **1997**, *106*, 8691.
(45) NIST Chemical Webbook, http://webbook.nist.gov, 2002.
(46) Hertl, M.; Jolly, J. *J. Phys. D: Appl. Phys.* **2000**, *33*, 381.
(47) Perrin, J. *J. Phys. D: Appl. Phys.* **1993**, *26*, 1662.
(48) Perrin, J.; Leroy, O.; Bordage, M. C. *Contrib. Plasma Phys.* **1996**, *36*, 3.
(49) Kessels, W. M. M.; Hoefnagels, J. P. M.; Boogaarts, M. G. H.; Schram, D. C.; Van de Sanden, M. C. M. *J. Appl. Phys.* **2001**, *89*, 2065.